



HAL
open science

Electron transfer properties of mono- and diferrocenyl based Cu complexes attached as self-assembled monolayers on gold electrodes by "self-induced" electroclick

Christophe Orain, Pascal Le Poul, Yves Le Mest, Nicolas Le Poul

► **To cite this version:**

Christophe Orain, Pascal Le Poul, Yves Le Mest, Nicolas Le Poul. Electron transfer properties of mono- and diferrocenyl based Cu complexes attached as self-assembled monolayers on gold electrodes by "self-induced" electroclick. *Journal of electroanalytical chemistry and interfacial electrochemistry*, 2013, 710, pp.48-58. 10.1016/j.jelechem.2013.02.014 . hal-00879630

HAL Id: hal-00879630

<https://univ-rennes.hal.science/hal-00879630>

Submitted on 9 Jan 2014

HAL is a multi-disciplinary open access archive for the deposit and dissemination of scientific research documents, whether they are published or not. The documents may come from teaching and research institutions in France or abroad, or from public or private research centers.

L'archive ouverte pluridisciplinaire **HAL**, est destinée au dépôt et à la diffusion de documents scientifiques de niveau recherche, publiés ou non, émanant des établissements d'enseignement et de recherche français ou étrangers, des laboratoires publics ou privés.

Electron transfer properties of mono- and diferrocenyl based Cu Complexes attached as self-assembled monolayers on gold electrodes by "self-induced" electroclick

Christophe Orain^a, Pascal Le Poul^b, Yves Le Mest^a, Nicolas Le Poul^{a,*}

^a*Chimie, Electrochimie Moléculaires et Chimie Analytique, UMR 6521 CNRS, Université de Bretagne Occidentale, 6 Avenue Le Gorgeu 29238 Brest Cedex 03, France*

^b*Organométalliques et Matériaux Moléculaires, UMR 6226 CNRS, Institut des Sciences Chimiques de Rennes, IUT BP 30219, 22302 Lannion Cedex, France*

Abstract

Two new Cu complexes bearing a 6-ethynyl bis-(methyl-pyridyl)amine (6eBMPA) moiety, as an electroclickable function linked to a ferrocenyl-based triazolyl arm (ligands **3** and **4**) have been synthesized and characterized by UV-Visible, EPR spectroscopies and cyclic voltammetry in acetonitrile. Two different spacer groups between the terminal ferrocene and the triazolyl group were inserted: an hexyl chain in the case of the complex Cu-**3**, an ethenyl-bridged diferrocenyl system for the complex Cu-**4**. The monoelectronic oxidation of the diferrocenyl species yields a stable mixed-valence complex. NIR-Visible spectroscopic studies show a moderate interaction between ferrocenyl units (class II according to the Robin-Day classification). The immobilization of these systems as SAMs on an azidoundecanethiol modified gold electrode has been successfully operated by using the "self-induced electroclick" procedure. The voltammetric characterization of the surface-tagged Cu complexes indicates that good surface coverage was achieved, with moderately fast electron-transfer reaction between the electrode and the redox active immobilized systems ($k^0(\text{Cu}) = 2\text{-}4 \text{ s}^{-1}$, $k^0(\text{Fc}) = 20\text{-}90 \text{ s}^{-1}$). Remarkably, the rate of charge transport is significantly controlled by the nature of the spacer on the ferrocenyl triazole arm.

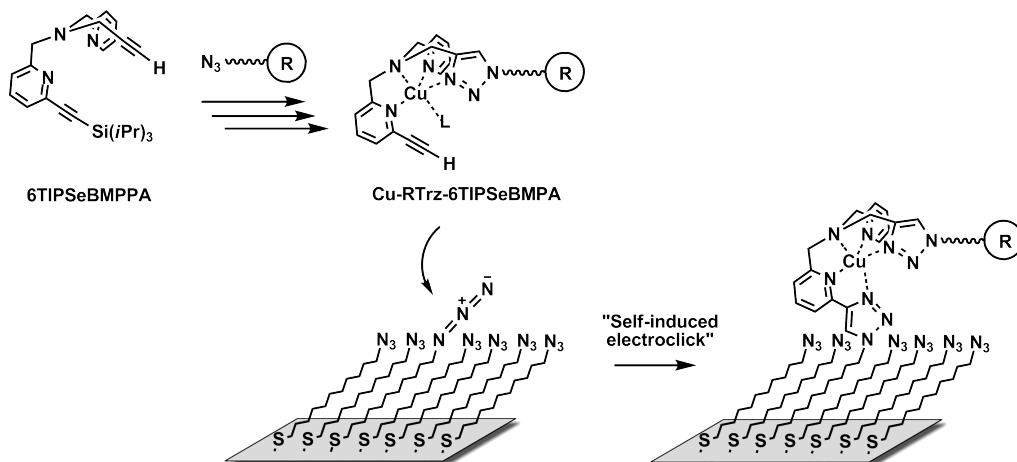
Keywords: Electrode functionalization, SAMs, click chemistry, copper, diferrocene, electron transfer kinetics, mixed-valence complex, QCA

1. Introduction

Ordered molecular assemblies based on organometallic compounds and coordination complexes display considerable interest in many fields such as electronic technology [1–3], biochemical and chemical sensing [4, 5], molecular catalysis and solar energy conversion [6, 7]. In particular, self-assembled monolayers (SAMs) of metallic-terminated alkanethiols on gold surfaces have been widely investigated and well-characterized by a large number of surface techniques [8, 9]. The best control of the surface organization is commonly obtained through procedures incorporating the prefunctionalization of the surface to prevent the formation of holes, especially in the case of sterically encumbered complexes [5, 10, 11]. Thanks to geometric/electronic properties under control of the coordination process, metallic complexes display a wide variety of properties as regards to complexation, redox, spin states... which infer to them versatile and tunable functionalities as compared to purely organic systems [8]. Particularly, SAMs of polynuclear metal complexes display promising properties. Hence, a recent study showed that multivalent interactions could improve the sensitivity of biosensors [12]. In the field of nanoelectronics, the incorporation of redox-active metallic centers into an organic backbone yields an enhancement of the charge transport over long distances [13, 14]. Probably one of the most promising domain concerns molecular Quantumdot Cellular Automata (QCA) [15, 16]. The general principle of QCA is to encode binary information in a cell composed of a small number of quantum dots. Each dot corresponds to a region in which the charge is localized in a nonbonding state, the electrostatic effect of neighboring cells inducing a Boolean state (1 or 0). In a cell, dots are separated to each other by tunneling pathways, such that a localized charge will induce a dipolar momentum in the cell. A significant coupling between the redox centers is also determining to permit rapid exchange of charge between the two sites. Pioneering works by Lent and Fehner have established that class I and II mixed-valence complexes in the Robin-Day classification [17] are the more promising candidates for molecular QCA cells [18–21]. Several symmetrical and unsymmetrical systems bearing ferrocenyl units have been immobilized as SAMs and tested for their QCA properties [19, 22–25]. Recently, three carbazole-bridged diferrocenyl complexes which display little conjugation between ferrocenyl

*corresponding author. tel.: +33 2 98 01 61 68

Email address: nicolas.lepoul@univ-brest.fr (Nicolas Le Poul)



Scheme 1: The self-induced electroclick strategy used for the immobilization of ferrocenyl and phenyl (R) derivatives onto non-mixed azidoundecanethiol modified gold electrodes.

units have been described [16]. They satisfied all important requirements for 6-dots QCA cells, particularly a low modification of the geometry with the redox state.

We have recently described a novel strategy for the immobilization of diverse functional objects on SAMs of azidoundecanethiol grafted on gold electrodes [26]. The procedure consists in two steps (Scheme 1): (i) a pre-functionalization of a 6TIPSeBMPPA generic platform (TIPS = triisopropylsilyl, eBMPPA = ethynyl-bis(methylpyridyl)propargylamine) by a molecular object of interest (R) through a Copper catalysed Azide-Alkyne Cycloaddition (CuAAC click reaction); (ii) an immobilization in aqueous media onto an azido-alkane modified gold electrode by using the self-induced electroclick approach [27] (Scheme 1). As preliminary trials, two different molecular objects were attached: one bearing a phenylpropyl (R=PhPr) group as a referring non-redox system, and the other a ferrocenylmethyl (R=FcMe) unit as an electrochemical probe [26]. The immobilization was operated by the *in situ* electrochemical reduction of the $[\text{Cu}^{\text{II}}\mathbf{1}(\text{L})_n]^{2+}$ and $[\text{Cu}^{\text{II}}\mathbf{2}(\text{L})_n]^{2+}$ ($\mathbf{1}$ =PhPrTrz-6eBMPPA, $\mathbf{2}$ =FcMeTrz-6eBMPPA, with Trz-6eBMPPA = triazolyl-6ethynyl-bis(methylpyridyl)amine) (Figure 1). A good surface coverage was achieved in both cases, the two systems displaying a moderately fast electron-transfer reaction between the electrode and the redox active immobilized complexes. Interestingly, the voltammetric study of the ferrocenyl-

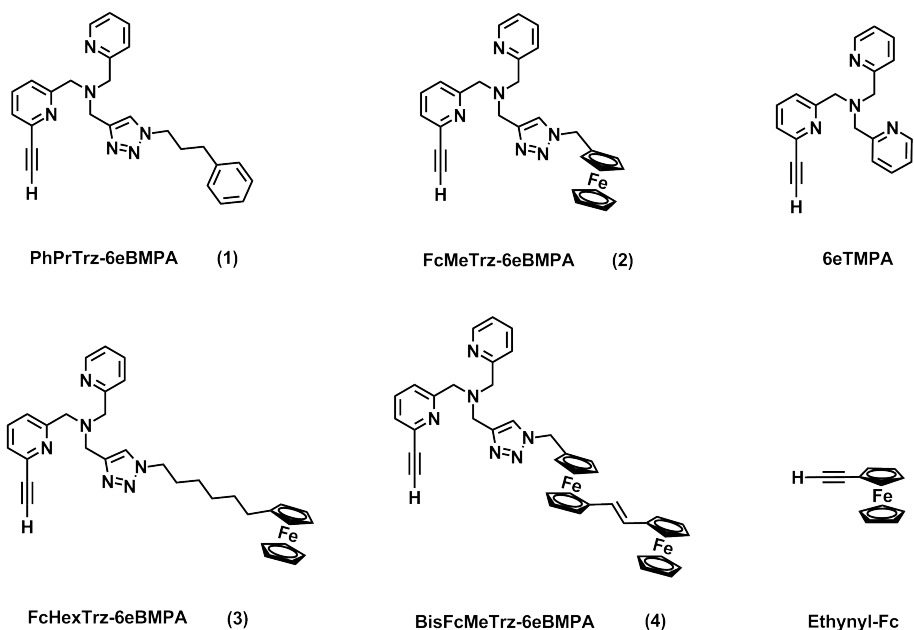


Figure 1: Schematic representation of Ligands (1-4), 6eTMPA and ethynylferrocene.

based Cu complex highlighted the significant effect of the copper ion on the kinetics of electron transfer. Hence, the removal of the metal ion induced a decrease of the electronic transfer rate which was interpreted as a structural modification of the N ligand attached on gold. Aiming to investigate the influence on the redox properties of the spacer connecting the Cu core to a redox center, we present in this work two novel ferrocenyl ligands which can be self-electroclicked onto azido modified electrodes as Cu complexes. In one case, the methyl spacer connecting the triazolyl group (Trz) to the terminal ferrocenyl unit **2** is lengthened to six carbons (FcHexTrz-6eBMPA, **3**) (Figure 1). In the second case, a 1,2-diferrocenylethenyl moiety (BisFcMeTrz-6eBMPA, **4**) (Figure 1) is the terminal unit. These ligands and their Cu complexes were fully characterized in solution by spectroscopic and electrochemical techniques. The complexes were immobilized as SAMs onto gold and studied by cyclic voltammetry at different scan rates. The influence of the spacer (size, partial conjugation) between the terminal ferrocene and the copper core on the thermodynamics and dynamics of the electron transfer was deeply investigated. The diferrocenyl compound **4** was also scrutinized at oxidation. The optical and electrochemical property

of the mixed-valence complex in solution, linked to the possibility to attach it in a controlled way onto gold surface may find some echoes in the design of new molecular QCA cells.

2. Experimental

Chemicals. Organic solvents were distilled on CaH_2 except THF and diethyl ether on Na/benzophenone. Acetonitrile (99.9% BDH, VWR) was used as received and kept under N_2 in the glovebox. All solvents were thoroughly degassed before use. NBu_4PF_6 was synthesized from NBu_4OH (Fluka) and HPF_6 (Aldrich). It was then purified, dried under vacuum for 48 hours at 100°C , then kept under N_2 in the glovebox. The compounds 6BrTMPA [28], PhPrN_3 [29] and FcMeN_3 [30] were prepared according to the literature. The synthesis of 11-azidoundecane-1-thiol was performed following a previously described procedure [31]. All other chemicals were of reagent grade and were used without purification.

Apparatus. Mass analyses (Electrospray-TOF) were performed by the "Service Central d'Analyses du CNRS", Solaize, France. NMR spectra were recorded on a Bruker DRX 500 MHz apparatus. IR spectra were recorded on a Vertex 70 ATR-FTIR Bruker instrument. EPR spectra were run on a Bruker Elexys spectrometer (X-band). UV-Visible-NIR spectroscopy was performed with a JASCO V-670 spectrophotometer.

Electrochemical experiments. The electrochemical studies in organic solvents were performed in a glovebox (Jacomex) ($\text{O}_2 < 1$ ppm, $\text{H}_2\text{O} < 1$ ppm) with a home-designed 3-electrodes cell. A commercial Pt removable tip electrode (Metrohm) was used as working electrode. Before each experiment, it was polished on a slurry with alumina ($3\ \mu\text{m}$) and sonicated in water (Millipore, $18\ \text{M}\Omega$). The counter-electrode was a platinum wire. A separate frit containing a Pt electrode dipping in an equimolar electrolytic solution of ferrocenium hexafluorophosphate (FcPF_6) and ferrocene (Fc) was used as the reference electrode. The potential of the cell was controlled by an AUTOLAB PGSTAT 302 (Ecochemie) potentiostat monitored by a computer and piloted with the NOVA software. In organic media, ferrocene was added at the end of each experiment to determine accurate redox potential values. Voltammetry in aqueous electrolytes was performed by using a standard calomel reference electrode (KCl saturated).

Electrode modification. A commercial gold removable tip electrode (Metrohm) was used. Before modification, the surface of the gold electrode ($A = 0.07\ \text{cm}^2$) was prepared following a classical procedure: after a polish

on a slurry with alumina ($3\ \mu\text{m}$), the electrode was sonicated in water (Millipore, $18\ \text{M}\Omega$) and cycled between 0.5 and 1.4 V vs SCE in H_2SO_4 0.1 M (40 scans) to remove gold oxide, washed with water, then ethanol and dried under slight flow of N_2 before being introduced in the solution containing the thiol compound. This procedure allowed the use of a same electrode with a appropriate resurrected Au surface condition. The electrode was kept in a non-mixed 1-azido-11-undecanethiol ($\text{N}_3(\text{CH}_2)_{11}\text{SH}$) 1 mM solution (solvent: EtOH) for 12 hours under N_2 . After thorough washing with pure EtOH, the electrode was tested by voltammetry in an aqueous solution of ferricyanide. The absence of redox signal indicated a blockage of the electron transfer at the electrode surface by the thiol compound.

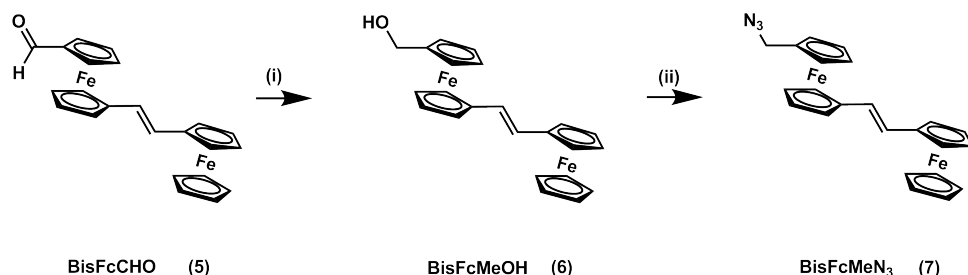
Complex immobilization. All Cu(**1-4**) complexes were immobilized onto an azidoundecanethiol-modified gold electrode by the "self-induced electroclick" procedure already described [26, 27]. The grafting of the complexes was achieved by cycling the potential between 0.60 V and -0.20 V with a 3 minutes hold at -0.20 V between each cycle in a $20\ \mu\text{M}$ ($50\ \mu\text{M}$ for Cu-**3**) aqueous solution of Cu complex. Acetonitrile was used as the co-solvent (1% volume) for the complexes since $[\text{Cu}^{\text{II}}\mathbf{3}(\text{L})_n]^{2+}$ and $[\text{Cu}^{\text{II}}\mathbf{4}(\text{L})_n]^{2+}$ are poorly soluble in water.

Ligands and complexes syntheses. Complementary details concerning the synthesis and characterization of ligands **3**, **3'**, **4**, **4'**, **6** and **7** (NMR, Mass spectrometry), as well as Cu-**3** and Cu-**4** (UV-Visible-NIR, EPR) are given in supplementary information part.

3. Results and discussion

3.1. Synthesis and characterization of the ligands and Cu complexes in solution

The synthesis of the 6TIPSeBMPPA generic platform, as well as both PhPrTrz-6eBMPA **1** and FcMeTrz-6eBMPA **2** ligands are described in ref. [26]. The $\text{Cu}^{\text{II}}\text{-1}$ and $\text{Cu}^{\text{II}}\text{-2}$ complexes were previously characterized by EPR, UV-vis spectroscopy and cyclic voltammetry. For the two novel ligands **3** and **4**, as a preliminary step, the ferrocenylhexylazide (FcHexN_3) and the bisferrocenylmethylazide (BisFcMeN_3) species were synthesized (see below). The ligands **3** and **4** were then prepared following the biphasic CuAAC procedure used for **1** and **2** (see ref. [26]).



Scheme 2: Synthetic pathway for the BisFcMe-N₃ compound (**7**): (i) NaBH₄ (6 equiv.), THF: methanol (1:2); 25 °C, 1 hour; (ii) NaN₃ (6 equiv.), acetic acid 80 °C, 3 hours.

3.1.1. Synthesis and characterization of the azide derivatives

The syntheses of the ferrocenylmethylazide [29], phenylpropylazide [30] and ferrocenylhexylazide [32] species (FcMeN₃, PhPrN₃ and FcHexN₃ respectively) were previously described. For the diferrocenyl derivative (**7**) (BisFcMeN₃), the mono-substituted aldehyde (**5**) (BisFcCHO) was first synthesized starting from the ferrocene according to a published procedure [33, 34]. The aldehyde was then reduced into the alcohol (**6**) (BisFcMeOH) by reaction with NaBH₄ [35]. This was followed by the azidation in presence of NaN₃ in glacial acetic acid to yield (**7**) (Scheme 2) [29]. The resulting complex was obtained as a mixture of diastereoisomers (Z:E, 1:9).

All four N₃ compounds were characterized by ¹H NMR (see experimental data) and FTIR spectroscopies. The N₃ vibration frequency values for the phenylpropylazide (PhPrN₃), ferrocenylmethylazide (FcMeN₃), ferrocenylhexylazide (FcHexN₃) and diferrocenylmethylazide (BisFcMeN₃) are respectively 2092, 2090, 2090, 2086 cm⁻¹. They are typical of organic azides [36].

3.1.2. Synthesis and characterization of the ligands (**1-4**)

The first step was operated by a biphasic CuAAC reaction involving the TIPS-protected BMPPA platform and the azido terminated species as previously described [26]. The resulting compounds bearing the TIPS protecting group (**1'-4'**) were characterized by NMR spectroscopy (see supporting information). The deprotection of the alkyne group was performed by reaction with tetrabutylammonium fluoride (NBu₄F) leading to the ethynyl ligands (**1-4**) (Figure 1). After purification by column chromatography on silica gel with CH₂Cl₂/MeOH as eluent, the ligands were fully characterized by ¹H, ¹³C NMR spectroscopies and single mass (ESI-TOF) spectrometry

(see supporting information). The ligands (**1-4**) were also studied by UV-Vis spectroscopy and voltammetry in acetonitrile. As shown in Table 1, their data have been compared to existing records on other mono and diferrocenyl species, as well as compounds (**5-7**).

As shown in Table 1, the redox potential of the monoferrocenyl species is fully controlled by the inductive effect of the substituting group. Indeed, the more electron withdrawing substituting group, the higher E^0 is (CHO > Ethynyl > MeN₃, MeTrz > MeOH, H > CH₃, HexTrz, HexSH). Such an effect can be attributed to the decrease of the electronic density on the ferrocenyl centre. On the other hand, the UV-Vis features (wavelength λ_{\max} and extinction coefficient ϵ_{\max}) seem slightly affected by the variation of the substituent. This is however not the case of the ferrocenylcarboxaldehyde compound (FcCHO) which displays higher values of λ_{\max} and ϵ_{\max} than the other monoferrocenyl species. This effect likely results from the conjugated character of the complex due the CHO moiety, as corroborated by the values obtained for the other conjugated ferrocenyl compounds (Table 1).

For the diferrocenyl species, the spectroscopic and voltammetric data show that the electronic properties are dictated not only by the withdrawing effect of the substituting group, but also by the monomeric or dimeric character of the substitution on both ferrocenyl groups, as well as the conjugated nature of the linker. Compound **4** bearing a vinyl spacer between mono-substituted and di-substituted ferrocenyl moieties, is a typical example. In UV-Vis, it absorbs at $\lambda_{\max} = 458$ nm, a value which is close to that found for other bis-ferrocenyl complexes bearing a vinyl spacer [38, 41]. The shift of the wavelength compared to the mono-ferrocenyl compounds is best explained by the presence of this spacer which allows an electronic conjugation, thus a decrease of the energy gap (i.e. an increase of λ_{\max}). This is accompanied by the increase of the extinction coefficient ϵ_{\max} . The maximum values are obtained for compound **5** which has the most conjugated system.

The electrochemical behaviors of compounds **4-7** are also informative about the electronic influence of the substituting groups on the diferrocenyl moieties. As the two ferrocenyl units are not equivalent (mono vs disubstituted), two reversible systems are systematically detected for each compound. The assignation of the redox potentials to each of the ferrocenyl unit can be proposed by comparison with other monoferrocenyl and diferrocenyl compounds (Table 1). For instance, for the BisFcCHO species (compound **5**, see Figure 2A), the system with the highest potential value

Table 1: UV-vis spectroscopic and voltammetric data for ligands **2-7** and other ferrocenyl-based compounds in acetonitrile (NBu₄PF₆ or KPF₆ 0.1 M).

Ferrocenyl derivative	λ_{\max} /nm (ϵ /M ⁻¹ cm ⁻¹)	E^0 /V vs Fc (ΔE_p /mV)
FcMeTrz-6eBMPA (2)	437 (170)	0.10 (90)
FcHexTrz-6eBMPA (3)	421 (280)	-0.07 (90)
BisFcMeTrz-6eBMPA (4)	458 (1700)	-0.02 (100), 0.21 (100)
BisFcCHO (5)	466 (1760)	-0.06 (100), 0.36 (90)
BisFcMeOH (6)	458 (1570)	-0.03 (65), 0.13 (70)
BisFcMeN ₃ (7)	458 (1260)	-0.02 (90), 0.19 (85)
FcMeN ₃	436 (100)	0.08 (75)
FcHexSH	439 (130)	-0.05 (75)
FcCHO	458 (570)	0.29 (80)
FcMeOH	439 (80)	0.00 (90)
Fc	441 (130)	0.00 (75)
MeFc		-0.06 ^a
EthynylFc	443 (130)	0.14 (80)
BisFc-ethene	458 (1450) ^{b,c}	-0.11, 0.03 ^{b,c}
BisFc-ethane		-0.07, 0.03 ^d

^a From ref. [37]; ^b From ref. [38] in CH₂Cl₂;

^c From ref. [39] in CH₂Cl₂; ^d From ref. [40].

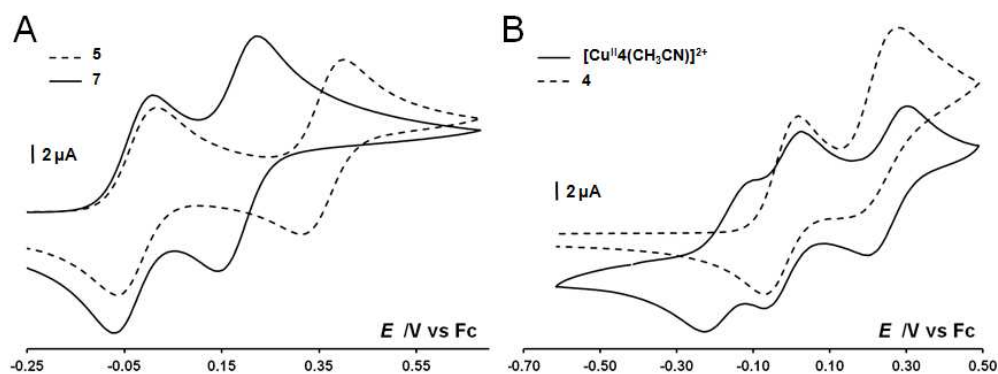


Figure 2: Cyclic voltammograms (E /V vs Fc) at a Pt electrode ($v = 0.1 \text{ V s}^{-1}$) in $\text{CH}_3\text{CN}/\text{NBu}_4\text{PF}_6$ 0.1 M of A) compounds **5** (dashed) and **7** (plain); B) compound **4** (dashed) and $[\text{Cu}^{\text{II}}\mathbf{4}(\text{L})_n]^{2+}$ (plain). $C = 1 \text{ mM}$.

($E^0 = 0.36 \text{ V}$) is undoubtedly ascribed to the disubstituted unit by analogy with the monoferrocenyl carboxaldehyde FcCHO ($E^0 = 0.29 \text{ V}$). On the other hand, the monosubstituted unit in **5** is oxidised at a lower potential value ($E^0 = -0.06 \text{ V}$), in the same range of potential than that of MeFc or FcHexSH . Correlatively, the two reversible systems detected for the bisferrocenyl-BMPA ligand **4** at $E^0 = -0.02 \text{ V}$ and $E^0 = 0.21 \text{ V}$ vs Fc can be ascribed to the mono- and disubstituted species respectively (Figure 2B). The higher value, $E^0 = 0.36 \text{ V}$, for the disubstituted moiety in compound **5**, as compared to those obtained for the three other diferrocenyl species **4**, **6** and **7** (Table 1), is explained by the lower electron withdrawing effect of the methyltriazole, methanol, or methylazide groups compared to the carboxaldehyde. At last, the E^0 value for the terminal monosubstituted ferrocene is significantly lower for **4** in comparison to **2**. Probably, the electron withdrawing effect of the triazole is no longer effective on the ferrocenyl center due to longer distance, as for the FcHexTrz-6eBMPA ligand (**3**). In conclusion, these data emphasize the influence of the environment around ferrocenyl units on the redox potential. It also allows to clearly discriminate between mono- and disubstituted moieties in diferrocenyl species, the latter displaying the highest redox potential values.

3.1.3. Cu complexation

The Cu complexes which can be electroclicked onto gold modified surfaces have been obtained by reaction of the unprotected ligands (**1-4**) with $\text{Cu}(\text{OTf})_2$ in acetonitrile. This complexation has been monitored by elec-

trochemistry or UV-Visible spectroscopy via successive addition of copper ion to avoid sub or over stoichiometry of Cu vs ligand. All Cu complexes were characterized by NIR-Visible and EPR spectroscopies and by cyclic voltammetry. The spectroscopic and voltammetric data are gathered in Table 2 and Table 3 respectively. As shown in Table 2, the analysis of the EPR spectra of the Cu complexes in CH₃CN yields $g_{\perp} < g_{//}$ factors and hyperfine constant values ($112 \text{ G} < A_{//} < 139 \text{ G}$). These latter values do not fit with typical values observed for a Cu complex in a square-based pyramidal (SBP) geometry such as for the Cu-6eTMPA complex ($A_{//} = 162 \text{ G}$), but more closely to those reported in the case of a tetrahedral (Td) distorted geometry [42–45].

Table 2: Spectroscopic data for the $[\text{Cu}^{\text{II}}(\mathbf{1-4})(\text{L})_n]^{2+}$ and $[\text{Cu}^{\text{II}}(6\text{eTMPA})(\text{L})_n]^{2+}$ complexes in CH₃CN.

Complex	$g(A/\text{G})$		$\lambda_{\text{max}} / \text{nm} (\epsilon / \text{M}^{-1} \text{ cm}^{-1})$	
	$g_{//}$	g_{\perp}	Fc	Cu($d-d$)
$[\text{Cu}^{\text{II}}\mathbf{1}(\text{L})_n]^{2+}$	2.23(112)	2.06		652(112)
$[\text{Cu}^{\text{II}}\mathbf{2}(\text{L})_n]^{2+}$	2.24(139)	2.06	437(196)	638(103),802(105)
$[\text{Cu}^{\text{II}}\mathbf{3}(\text{L})_n]^{2+}$	a	a	413(344)	658(123)
$[\text{Cu}^{\text{II}}\mathbf{4}(\text{L})_n]^{2+}$	2.21(117)	2.06	456(124)	648(133),804(126)
$[\text{Cu}^{\text{II}}(6\text{eTMPA})(\text{L})_n]^{2+}$	2.24(162) ^b	2.05 ^b		640(104),809(152) ^b

^a Not determined; ^b From ref. [27].

Table 3 presents the voltammetric data obtained for Cu(**1-4**) complexes in acetonitrile. All complexes display a reversible one-electron Cu(II)/Cu(I) process at very close standard potential values (-0.16 to -0.18 V vs Fc). This potential is higher than that of the Cu^{II}-6eTMPA complex in the same experimental conditions [27]. This indicates first that the coordinating environment is similar for all Cu(**1-4**) complexes. However the origin of the potential value difference with the Cu-6eTMPA complex is difficult to rationalize. Indeed, TMPA and BMPA Cu complexes differ by the presence of a sterically encumbered triazolyl group instead of a pyridyl group. Therefore, the increase of the redox potential for BMPA may be due to the combination of several effects: electronic (uncoordination of one coordinating arm),

steric (protection from the solvent medium which destabilizes the Cu(II) vs Cu(I) species) or geometric (a tetrahedral geometry destabilizes the Cu(II) complex and stabilizes the Cu(I) species). Another interesting point in the voltammetric data is the redox potential value for the ferrocenyl moieties. The Cu-**2** complex exhibits a slightly more positive value than the ligand **2** (+0.10 V vs +0.14 V respectively) (Table 1). Interestingly, this effect is very small for the Cu-**3** complex, indicating that the Lewis acidity of the Cu²⁺ affects only ferrocenyl groups in close contact. This is confirmed by the data obtained for the diferrocenyl complex Cu-**4**: only E^0 related to the disubstituted ferrocene is varied (0.21 V to 0.25 V) in presence of Cu²⁺ (whereas the standard potential of the terminal ferrocene is kept at -0.02 V, see Figure 2B).

Table 3: Voltammetric data for the [Cu^{II}(**1-4**)(L)_n]²⁺ and [Cu^{II}(6eTMPA)(L)_n]²⁺ complexes in CH₃CN/NBu₄PF₆ 0.1 M.

Complex	E^0 /V vs Fc (ΔE_p /mV)	
	Cu	Fc
[Cu ^{II} 1 (L) _n] ²⁺	-0.17 (90)	
[Cu ^{II} 2 (L) _n] ²⁺	-0.18 (115)	0.14 (90)
[Cu ^{II} 3 (L) _n] ²⁺	-0.18 (100)	-0.06 (90)
[Cu ^{II} 4 (L) _n] ²⁺	-0.16 (90)	-0.02 (90), 0.25 (90)
[Cu ^{II} (6eTMPA)(L) _n] ²⁺	-0.33 (65) ^a	

^a From ref. [27].

3.2. One and two-electron oxidation of the diferrocenyl Cu complex: characterization of a mixed-valence species in solution.

Alkene-bridged diferrocenyl compounds have been extensively studied as typical examples of dimeric species with electronic delocalization [39, 46–49]. When the two ferrocenyl units are equivalent, the through-bridge interaction between the two units is commonly quantified on the basis of the stability of the [Fc⁺-Fc] mixed-valence species. This is done by measuring the difference of standard potentials between each ferrocene (ΔE^0) when the

two- electron transfer is splitted into two one-electron systems. The resulting free energy is then directly correlated to the thermodynamic constant (K_{disp}) associated with the disproportionation reaction of the mixed-valence compound according to the equation (1) [47, 50]:

$$K_{\text{disp}} = \exp \left[\frac{F \Delta E^0}{RT} \right] \quad (1)$$

Here, the K_{disp}^{-1} constant can be considered as a measure of the degree of interaction between the redox centers through the unsaturated molecular bridge. It remains however a rough approximation as the electrostatic repulsion as well the solvent stabilization (which can give rise to potential inversion [51]) are not taken into account. According to the K_{disp} value, the mixed-valence species can be ranked into class I, II or III in the Robin-Day classification [17, 52]. For $[\text{Cu}^{\text{II}}\mathbf{4}(\text{L})_n]^{2+}$, the two ferrocenyl units are non-equivalent since they are mono and disubstituted. Thus, the strength of the interaction between the two centers can not be determined on the only basis of the standard potential difference value (ΔE^0). However, it can be estimated from the intervalence charge transfer (IVCT) band of the mixed-valence species typically observed in the NIR domain (900-2000 nm)[52]. In that purpose, the tricationic mixed-valence $[\text{Cu}^{\text{II}}\mathbf{4}(\text{L})_n]^{3+}$ ion was prepared by electrolysis of the dicationic $[\text{Cu}^{\text{II}}\mathbf{4}(\text{L})_n]^{2+}$ complex at a potential between the two ferrocenyl systems. Such species is stable in acetonitrile under inert atmosphere as shown by rotating-disk electrode voltammetry (Figure 3A, curve b). For comparison, the second oxidation was also performed to yield the tetracationic complex $[\text{Cu}^{\text{II}}\mathbf{4}(\text{L})_n]^{4+}$ (Figure 3, curve c).

UV-Visible-NIR spectroscopic studies were then performed on the di-, tri- and tetracationic species. As shown in Figure 3B, the successive oxidations of the $[\text{Cu}^{\text{II}}\mathbf{4}(\text{L})_n]^{2+}$ complex lead to a red-shift of the maximum wavelength (λ_{max}) related to the Metal to Ligand Charge Transfer (MLCT) transition, as well as a decrease of the corresponding molar extinction coefficient (ϵ_{max}) [456 nm ($1150 \text{ L mol}^{-1} \text{ cm}^{-1}$), 528 nm ($790 \text{ L mol}^{-1} \text{ cm}^{-1}$), 636 nm ($315 \text{ L mol}^{-1} \text{ cm}^{-1}$) for the 2^+ , 3^+ and 4^+ species respectively]. The modification of the spectrum with the increase of the oxidation state corresponds to a decrease of the HOMO-LUMO energy gap, as typically observed for the ferrocenium/ferrocene couple. The wavelength value found for the tricationic species (528 nm), lying between those of the dicationic and the tetracationic, is indicative of the delocalizing character of the linker. The

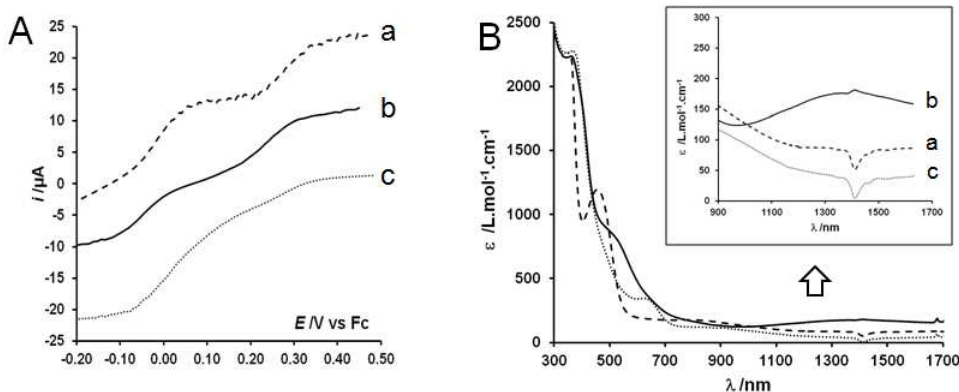


Figure 3: A) Rotating-disk electrode voltammograms of $[\text{Cu}^{\text{II}}\mathbf{4}(\text{L})_n]^{2+}$ in $\text{CH}_3\text{CN}/\text{NBu}_4\text{PF}_6$ before (a) and after electrolysis at 0.10 V vs Fc (b) and 0.40 V vs Fc (c). B) Response in NIR-Vis spectroscopy of the $[\text{Cu}^{\text{II}}\mathbf{4}(\text{L})_n]^{4+}$ complex before (a) and after electrolysis (b and c).

decrease of ϵ_{max} with the oxidation state of the Fc moieties likely results from the decrease of the electronic density on the metal.

The NIR part of the spectra clearly shows the formation of an IVCT transition in the 900 nm to 1700 nm wavelength range for the tricationic species. For symmetrical systems, the IVCT transition yields to the determination of the electronic coupling, H_{ab} , according to the equation (2) [47, 53, 54]:

$$H_{\text{ab}} = \left[\frac{0.0206}{r_{\text{ab}}} \right] [\epsilon_{\text{max}} \nu_{\text{max}} \Delta\nu_{1/2}]^{1/2} \quad (2)$$

[r_{ab} is the distance (\AA) between the two centers without electronic coupling, ϵ_{max} ($\text{L Mol}^{-1} \text{cm}^{-1}$) and ν_{max} (cm^{-1}) are the maximum molar coefficient and frequency values for the IVCT band respectively, $\Delta\nu_{1/2}$ is the mid-height width (cm^{-1})].

Hush's theory predicts for such systems that the theoretical value of $\Delta\nu_{1/2}$ ($\Delta\nu_{1/2\text{theo}}$) can be determined from ν_{max} since:

$$(\Delta\nu_{1/2})_{\text{theo}} = [2310 \times \nu_{\text{max}}]^{1/2} \quad (3)$$

The ratio of the experimental value to the theoretical one yields the Γ parameter as shown by the equation (4):

$$\Gamma = 1 - \frac{\Delta\nu_{1/2}}{(\Delta\nu_{1/2})_{\text{theo}}} \quad (4)$$

The value found for Γ is a good indicator of the degree of electronic delocalization. For instance, weakly coupled systems of class II are characterized by Γ values between 0 and 0.1. As the electronic delocalization is increased from class II to class III, the Γ factor is increased ($\Gamma > 0.5$ for class III) [47, 52].

Strictly, these equations are not valid for unsymmetrical systems such as $[\text{Cu}^{\text{II}}\mathbf{4}(\text{L})_n]^{2+}$. However, the value of $(\Delta\nu_{1/2})_{\text{theo}}$ can be approximated by incorporation of the difference in free energy between each center (ΔG^0 in cm^{-1}) in the calculations [55]:

$$(\Delta\nu_{1/2})_{\text{theo}} = [2310 \times (\nu_{\text{max}} - \Delta G^0)]^{1/2} \quad (5)$$

with

$$\Delta G^0 = 8065.54 \times \Delta E^0 \quad (6)$$

and

$$\lambda = \nu_{\text{max}} - \Delta G^0 \quad (7)$$

where λ is the reorganizational energy associated with the electron transfer reaction.

For $[\text{Cu}^{\text{II}}\mathbf{4}(\text{L})_n]^{2+}$, the analysis of the experimental data of the IVCT transition gives $\nu_{\text{max}}=7256 \text{ cm}^{-1}$, $\epsilon_{\text{max}}=132 \text{ L mol}^{-1} \text{ cm}^{-1}$ and $\Delta\nu_{1/2}=2217 \text{ cm}^{-1}$. The distance between the two ferrocenyl units is assumed to be 7 Å from the center-to-center distance value for the diferrocenyl ethene in a *trans* configuration [38]. The potential difference value (ΔE^0) can be estimated by considering only units without alkene linker. It is calculated from the difference of redox potential in acetonitrile related to the ferrocenyl unit in $[\text{Cu}^{\text{II}}\mathbf{2}(\text{L})]^{2+}$ and ferrocene.

From these values, the equations (2) and (7) lead to the determination of H_{ab} and λ (136 cm^{-1} and 6127 cm^{-1} respectively) for $[\text{Cu}^{\text{II}}\mathbf{4}(\text{L})_n]^{2+}$. The value found for H_{ab} is comparable to the reported data for weakly-coupled diferrocenyl mixed-valence complexes [38, 41, 55]. Equation (5) allows the determination of the theoretical bandwidth value ($(\Delta\nu_{1/2})_{\text{theo}} = 3762 \text{ cm}^{-1}$). The degree of the electronic delocalization (Γ) can thus be evaluated by using equation (4). The calculated value ($\Gamma = 0.41$) indicates that the complex displays a moderate electronic delocalization and hence belongs to the class II in the Robin-Day classification. The comparison between the electronic

constant and half of the reorganizational energy values ($H_{ab} < \lambda/2$) confirms the class II character of the interaction [55]. In conclusion, these data indicate that the redox splitting of the two Fc^+/Fc processes observed by cyclic voltammetry [$\Delta E^0 = 0.25 - (-0.02) = 0.27$ V] for $[\text{Cu}^{\text{II}}\mathbf{4}(\text{L})_n]^{2+}$ results from the combination of moderate electronic delocalization through the alkene linker, as well as from the difference of substitution (mono- vs di-) of the two ferrocenyl moieties.

3.3. Immobilization of the Cu complexes onto gold modified electrodes

The Cu(**1-4**) complexes were attached onto an azidoundecanethiol modified gold electrode by the "self-induced electroclick" method (see experimental part for details). As shown in Figure 4 for $[\text{Cu}^{\text{II}}\mathbf{4}(\text{L})_n]^{2+}$, three systems at 0.06 V, 0.33 V and 0.48 V vs SCE appeared clearly as the cycling was performed. The increase of the current intensities indicated that the immobilization of the complex occurred on the electrode surface. After 16 cycles, the intensity of the peaks reached a maximum value, suggesting that all available azido sites were clicked. Plots of surface coverage vs time for the Cu(II) reduction process for each cycle yielded the kinetics of triazole formation on the surface, as previously done for $[\text{Cu}^{\text{II}}\mathbf{1}(\text{L})_n]^{2+}$ and $[\text{Cu}^{\text{II}}\mathbf{2}(\text{L})_n]^{2+}$ [26].

As shown in Figure 4 (inset), a decay shape was obtained which fits reasonably well with a first order kinetic law (dashed line). The first-order (k'_{graft}) and second-order rate constant values ($k_{\text{graft}} = k'_{\text{graft}}/[\text{Cu}]$) for surface immobilization of the $[\text{Cu}^{\text{II}}\mathbf{4}(\text{L})_n]^{2+}$ were determined assuming that the ethynyl complex was in excess vs azido groups. The same procedure was used for the other Cu complexes as well as the ethynylferrocene compound. All k'_{graft} and k_{graft} values are gathered in Table 4. This data clearly shows that the self-induced electroclick procedure yields similar rates of grafting for this series of complexes in comparable experimental conditions ($k'_{\text{graft}} = 1.2$ to 2.8 s^{-1}). The slight differences between immobilization rates may be due to the combination of electronic or steric effects. The latter are likely predominant since all Cu complexes (except Cu-6eTMPA) display similar reduction potential in acetonitrile (see Table 3). Another interesting point in Table 4 concerns the kinetics of grafting for the ethynylferrocene ($k'_{\text{graft}} = 3.5$ s^{-1} , $k_{\text{graft}} = 140$ $\text{M}^{-1} \text{s}^{-1}$,) when using 25 μM of Cu catalyst ($[\text{Cu}^{\text{II}}(\text{6BrTMPA})(\text{H}_2\text{O})]^{2+}$). This value is 7 times lower than that previously found by Chidsey *et al.* [56]. Such difference may originate from the nature of the Cu catalyst, its concentration (400 μM) and the solvent (DMSO:H₂O, 3:1).

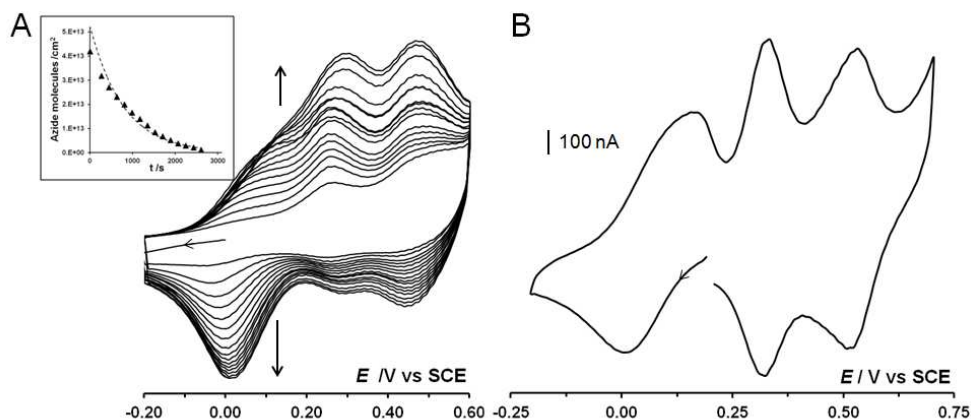


Figure 4: A) Cyclic voltammograms (16 cycles) at a $\text{N}_3(\text{CH}_2)_{11}\text{SH}$ modified Au electrode ($v = 0.1 \text{ V}\cdot\text{s}^{-1}$) of a solution of $[\text{Cu}^{\text{II}}\mathbf{4}(\text{L})_n]^{2+}$ ($20 \mu\text{M}$) in $\text{H}_2\text{O}/\text{KNO}_3$ 0.1 M under N_2 . Inset: plots of available azide molecules/ cm^2 vs time (seconds) for the Cu system from the variation of the surface coverage with time. Dashed line: exponential trend curve; B) Cyclic voltammograms ($v = 0.1 \text{ V s}^{-1}$) under N_2 in a 0.05 M buffer acetate solution (pH=4.5) + NaBF_4 0.05 M of the $[\text{Cu}^{\text{II}}\mathbf{4}(\text{L})_n]^{2+}$ complex grafted on the gold electrode.

After the grafting process, the Cu(**1-4**) modified gold electrodes were washed thoroughly with distilled water and then studied by cyclic voltammetry in an electroactive-free sodium-acetate-buffered solution (pH = 4.5) with NaBF_4 (0.05 M) as supporting electrolyte. This pH value was chosen as it is sufficiently low to stabilize the ferrocenyl unit, and sufficiently high to inhibit Cu demetallation by pyridyl protonation. All grafted complexes were studied at different scan rate. They exhibit linear variation of the peak current intensities (i_p) with scan rate, as expected for immobilized redox systems (see supplementary information).

As shown in Figure 5 and ref. [26], both monoferrocenyl Cu-**2** and Cu-**3** complexes display two reversible redox systems (see Table 5). As discussed previously, the Cu(II)/Cu(I) process occurs at the lowest potential (0.04 V vs SCE) whereas the Fc^+/Fc reaction takes place at a higher potential (*ca* 0.40 V vs SCE). When compared to the other complexes (excepted Cu-6eTMPA), the Cu(II)/Cu(I) redox potential does not change even if the triazole arm linked to the BMPA core is modified. Its value is also 100 mV higher than that obtained for $[\text{Cu}^{\text{II}}(\text{6eTMPA}(\text{H}_2\text{O}))_2]^{2+}$. Thus the

Table 4: First-order (k'_{graft}) and second-order (k_{graft}) rate constant values for the reaction of immobilization of $[\text{Cu}^{\text{II}}(\mathbf{1-4})(\text{L})_n]^{2+}$, $[\text{Cu}^{\text{II}}(6\text{eTMPA})(\text{L})_n]^{2+}$ and ethynylferrocene complexes from the CV analysis.

Complex	$10^3 k'_{\text{graft}}/\text{s}^{-1}$		$k_{\text{graft}}/\text{M}^{-1}\text{s}^{-1}$	
	Cu	Fc	Cu	Fc
$[\text{Cu}^{\text{II}}\mathbf{1}(\text{L})_n]^{2+}$	1.2		60	
$[\text{Cu}^{\text{II}}\mathbf{2}(\text{L})_n]^{2+}$	3.2	3.6	180	160
$[\text{Cu}^{\text{II}}\mathbf{3}(\text{L})_n]^{2+}$	1.5 ^a	b	30 ^a	b
$[\text{Cu}^{\text{II}}\mathbf{4}(\text{L})_n]^{2+}$	1.3	b	55	b
$[\text{Cu}^{\text{II}}(6\text{eTMPA})(\text{L})_n]^{2+}$	2.0		100	
EthynylFc		3.5 ^c		140 ^c

^a Performed with a 50 μM solution of the complex;

^b Undetermined value;

^c Performed with $[\text{Cu}^{\text{II}}(6\text{BrTMPA})(\text{H}_2\text{O})]^{2+}$ as precursor of catalysis (20 μM).

general trends obtained for the series with the Cu complexes being freely diffusing in acetonitrile (Table 3) are also observed in aqueous electrolyte with the complexes immobilized on the electrode surface immersed. The discrimination between electronic (i.e. number of N groups coordinated to Cu), geometric and steric effects is again not straightforward. At least, this data suggests that the coordinating environment around Cu is similar for all Cu-BMPA complexes. Since we showed by kinetics measurements that the demetallation of Cu-**2** by ammonia leads to a strong structural release of the arms [26], we believe that the triazole of the ferrocenyl arm is coordinated to the Cu ion as shown by the standard rate constant values for all complexes (see kinetic studies below). The ferrocene oxidation reaction for the grafted complexes was also investigated. Contrary to the Cu(II)/Cu(I) system, the redox potential for this process varies significantly with the nature of the arm as already observed for the ligands and the Cu complexes freely diffusing in acetonitrile (*vide infra*). Indeed the lowest E^0 values are obtained for the hexyl-Fc Cu-**3** complex (0.34 V vs SCE), as well as the

terminal ferrocenyl group of the diferrocenyl Cu-**4** complex (0.33 V). The maximum value is obtained for the disubstituted ferrocenyl unit of Cu-**4** (0.48 V), whereas the methyl-Fc Cu-**2** complex exhibits moderate standard potential (0.42 V). All systems are characterized by a good reversibility ($\Delta E_p < 30$ mV) and show fast electron transfer reaction for this process. The $\Delta E_{p,1/2}$ parameter is also close to 100 mV (at $v = 0.1$ V s⁻¹) except for the disubstituted ferrocenyl unit of Cu-**4** (150 mV). This latter effect may result from cross interactions between redox centers.

Table 5: Standard potential (E^0) and half-peak width ($\Delta E_{p,1/2}$) values for the grafted $[\text{Cu}^{\text{II}}(\mathbf{1-4})(\text{L})_n]^{2+}$, $[\text{Cu}^{\text{II}}(6\text{eTMPA})(\text{L})_n]^{2+}$ and ethynylferrocene complexes from the analysis of the cyclic voltammetry data obtained in a 0.05 M buffer acetate solution (pH=4.5) + NaBF₄ 0.05 M.

Complex	E^0 /V vs SCE		$\Delta E_{p,1/2}$ /mV	
	Cu ^{II/I}	Fc ⁺ /Fc	Cu ^{II/I}	Fc ⁺ /Fc
$[\text{Cu}^{\text{II}}\mathbf{1}(\text{L})_n]^{2+}$	0.04(42)		130	
$[\text{Cu}^{\text{II}}\mathbf{2}(\text{L})_n]^{2+}$	0.04(67)	0.42(10)	152	94
$[\text{Cu}^{\text{II}}\mathbf{3}(\text{L})_n]^{2+}$	0.05(70)	0.34(20)	120 ^a	91
$[\text{Cu}^{\text{II}}\mathbf{4}(\text{L})_n]^{2+}$	0.06(110)	0.33(20), 0.48(30)	198	108,150
$[\text{Cu}^{\text{II}}(6\text{eTMPA})(\text{L})_n]^{2+}$	-0.05(21)		133	
EthynylFc		0.44(15)		90

^a From the oxidation peak (171 mV for the reduction peak).

The experimental surface coverage (Γ_s) values of the Cu and Fc centers were then determined on the basis of two methods: (i) by integration of the CV peak current at low scan rate (the peaks were deconvoluted in the case of Cu-**3** and Cu-**4**, see supplementary information part for details), and (ii) by using the equation (8) assuming a reversible (fast) electron transfer for the reaction in the time domain [57]:

$$i_p = \frac{n^2 F^2}{4RT} v A \Gamma_s \quad (8)$$

[i_p is the current intensity, n is the number of electrons exchanged, A is the electrode surface area, Γ_s is the surface coverage, F is the Faraday constant, v is the scan rate, R is the perfect gas constant and T is the temperature].

As shown in Table 6, a decrease of Γ_s is observed for the most sterically encumbered species such as Cu-**3** and Cu-**4**. Indeed, as ferrocenyl groups are tagged to the BMPA core, and/or the length of the triazole arm is increased, the whole size of the species is increased, inversely to the coverage. To rationalize the effect, we calculated the theoretical values ($\Gamma_{s,theo}$) by assuming the species as an ellipsoid of defined diameters (see supplementary information part for details). If one excludes the Cu-**3** complex, the $\Gamma_s/\Gamma_{s,theo}$ ratio is close to 80 % (see Table 6). This indicates that the size of the species is indeed the main factor controlling the surface coverage.

Table 6: Experimental surface coverage (Γ_s /pmol cm⁻²), theoretical surface coverage ($\Gamma_{s,theo}$ /pmol cm⁻²) and $\Gamma_s/\Gamma_{s,theo}$ ratio (%) for the grafted [Cu^{II}(**1-4**)(L)_n]²⁺, [Cu^{II}(6eTMPA)(L)_n]²⁺ and ethynylferrocene complexes from the analysis of the cyclic voltammetry data obtained in a 0.05 M buffer acetate solution (pH=4.5) + NaBF₄ 0.05 M.

Complex	Γ_s		$\Gamma_{s,theo}$	$\Gamma_s/\Gamma_{s,theo}$	
	Cu ^{II/I}	Fc ⁺ /Fc		Cu ^{II/I}	Fc ⁺ /Fc
[Cu ^{II} 1 (L) _n] ²⁺	150 ^a , 120 ^b		190	79 ^c	
[Cu ^{II} 2 (L) _n] ²⁺	110 ^a , 80 ^b	160 ^a , 120 ^b	110	100 ^c	145 ^c
[Cu ^{II} 3 (L) _n] ²⁺	10 ^a , 20 ^b	10 ^a , 25 ^b	80	13 ^c	13 ^c
[Cu ^{II} 4 (L) _n] ²⁺	60 ^a , 50 ^b	70 ^a , 100 ^b	80	75 ^c	88 ^c
[Cu ^{II} (6eTMPA)(L) _n] ²⁺	160 ^a , 90 ^b		190	84 ^c	
EthynylFc	280 ^a , 210 ^b		360	78 ^c	

^a Calculated from the integration of CV peaks at $v = 0.1$ V s⁻¹;

^b Calculated from the slope $i_p = f(v)$ assuming the reversible case;

^c Calculated from the value of Γ_s obtained by integration of the CV peak.

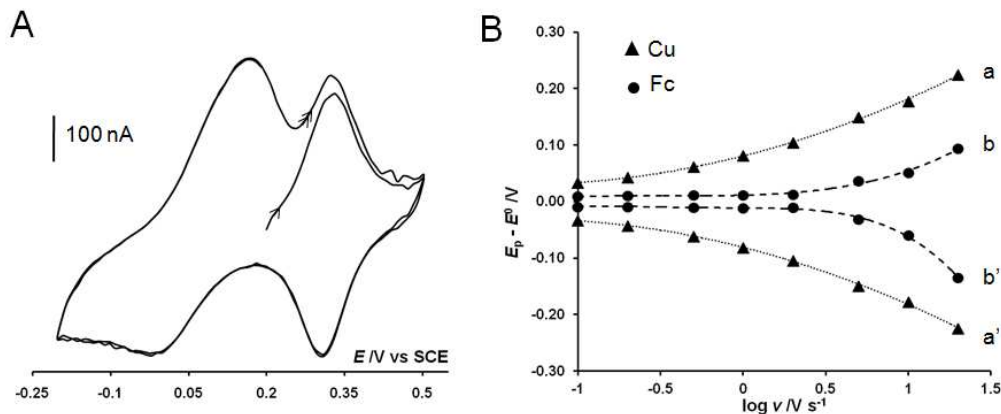


Figure 5: A) Cyclic voltammograms (2 cycles, $v = 0.5 \text{ V s}^{-1}$) of Cu-**3** grafted on a $\text{N}_3(\text{CH}_2)_{11}\text{SH}$ modified Au electrode under N_2 in a 0.05 M buffer acetate solution (pH=4.5) + NaBF_4 0.05 M. B) Plots of $(E_{\text{pa}} - E^0)$ (a, b) and $(E_{\text{pc}} - E^0)$ (a', b') vs $\log(v)$ ($0.1 \text{ V s}^{-1} < v < 20 \text{ V s}^{-1}$) from CVs of Cu-**3** grafted on a $\text{N}_3(\text{CH}_2)_{11}\text{SH}$ modified Au electrode under N_2 in a 0.05 M buffer acetate solution (pH=4.5) + NaBF_4 0.05 M. Triangle and disks depict the $\text{Cu}^{\text{II}}/\text{Cu}^{\text{I}}$ (a, a') and Fc^+/Fc (b, b') electron transfer processes, respectively.

3.4. Kinetics of the electron transfer for the Cu complexes-modified electrodes

Our previous kinetic studies on $[\text{Cu}^{\text{II}}(\text{6eTMPA})(\text{L})_n]^{2+}$, $[\text{Cu}^{\text{II}}\mathbf{1}(\text{L})_n]^{2+}$ and $[\text{Cu}^{\text{II}}\mathbf{2}(\text{L})_n]^{2+}$ immobilized onto an azidoundecanethiol modified gold electrode showed that the electron transfer rate for the $\text{Cu}(\text{II})/\text{Cu}(\text{I})$ system ($4 < k^0 < 10 \text{ s}^{-1}$) is significantly lower than that obtained for the Fc^+/Fc reaction ($k^0 = 90 \text{ s}^{-1}$). The dematallation of the Cu complex moiety by addition of ammonia leads to a large decrease of the ferrocenyl-related rate constant ($k^0 = 7 \text{ s}^{-1}$) [26]. This result suggested that the copper ion has essentially a structural role in the electron transfer process. In the present study, we specifically focused on the new complexes Cu-**3** and Cu-**4** to rationalize the effect of the spacer (Figure 5 and Figure 6). The kinetic study relies on the simple model developed by Laviron for immobilized redox centres [58]. This model allows the determination of the standard rate constant k^0 from high scan rate voltammetry, with the assumption that the redox centres are non-interacting between each others, and that the kinetics is not too fast ($< 10^3 \text{ s}^{-1}$). A more elaborated model which takes

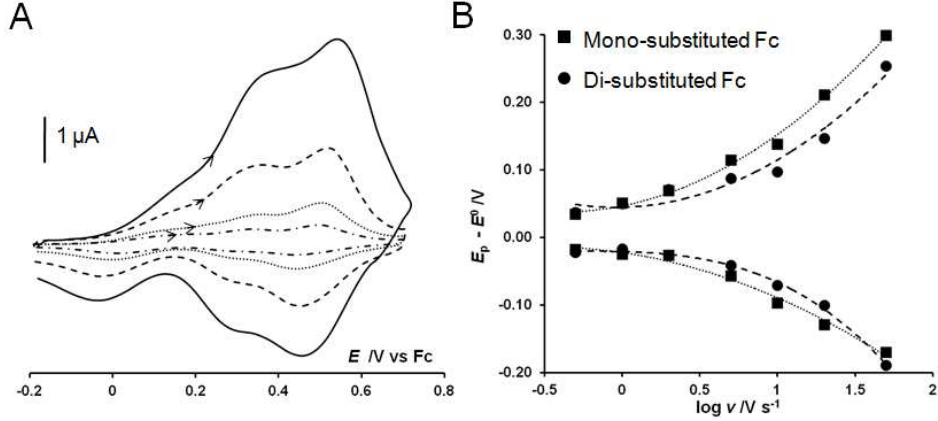


Figure 6: A) Cyclic voltammograms at variable scan rate of Cu-4 grafted on a $\text{N}_3(\text{CH}_2)_{11}\text{SH}$ modified Au electrode under N_2 at different scan rates in a 0.05 M buffer acetate solution (pH=4.5) + NaBF_4 0.05 M : $v = 0.1 \text{ V s}^{-1}$ (dot-dashed), 0.2 V s^{-1} (dot), 0.5 V s^{-1} (dashed), 1 V s^{-1} (plain). B) Plots of $(E_p - E^0)$ vs $\log(v)$ ($0.5 \text{ V s}^{-1} < v < 50 \text{ V s}^{-1}$) for the Fc^+/Fc processes from CVs of Cu-4 grafted on a $\text{N}_3(\text{CH}_2)_{11}\text{SH}$ modified Au electrode under N_2 in a 0.05 M buffer acetate solution (pH=4.5) + NaBF_4 0.05 M. Square and disks depict the Fc^+/Fc reaction for the mono- and disubstituted units, respectively.

into account cross interactions between centers was developed by Laviron et al. [59], but it was considered in the present study. When the scan rate is sufficiently high, such that the electron transfer reaction becomes the rate limiting process, one typically observes the linear increase of the peak separation (ΔE_p) with $\log(v)$. In that particular situation, Laviron predicts that the standard rate constant can be determined from the intercept for plots of ΔE_p vs $\log(v)$, according to the equation (9):

$$\Delta E_p = \left[\frac{2.3}{\alpha \beta n f} \right] \{ \alpha \log \beta + \beta \log \alpha + \log f - \log k^0 + \log v \} \quad (9)$$

[α is the symmetry barrier coefficient, n is the number of electrons involved, f is equal to F/RT , β equals $1 - \alpha$].

From the equation (9), the symmetry coefficient α has to be known to access k^0 . This is usually performed by plotting $(E_{pa} - E^0)$ and $(E_{pc} - E^0)$ vs $\log(v)$ (instead of ΔE_p). The intercepts of the linear part of the curves at high v with horizontal axis (E^0) yield $\log(v_a)$ and $\log(v_c)$ values. The α

coefficient is then calculated according to the equation (10):

$$\frac{\alpha}{1 - \alpha} = \frac{v_a}{v_c} \quad (10)$$

When the electron-transfer rate-limiting case cannot be reached (usually for $\Delta E_p < 200$ mV), it is possible to estimate k^0 from the equation (11), m^{-1} being calculated from ΔE_p values with $\alpha = 0.5$:

$$m = \frac{RTk^0}{nF} \quad (11)$$

Table 7 gives the standard rate constant values for each redox system in each complex. The electron transfer related to the Cu(II)/Cu(I) system in the case of the Cu(**1-4**) complexes is moderately fast ($k^0 \leq 4$ s⁻¹). It slightly decreases as the length of the triazole arm is increased, as shown by the lowest values obtained found for the grafted [Cu^{II}**3**(L)]²⁺ and [Cu^{II}**4**(L)]²⁺ complexes. Such effect is putitatively associated with the reorganizational energy (λ) necessary to accommodate the electron transfer, as usually observed for Cu systems when freely diffusing in solution. The high value found for the less sterically encumbered [Cu^{II}(6eTMPA)(L)]²⁺ complex seems to be in agreement with such a proposal.

The standard rate constants were also determined using the same procedure for the ferrocenyl units. As shown in Table 7, they are all at least 10 times higher than those found for the Cu(II)/Cu(I) redox system. This can be ascribed to a strong difference in reorganizational energies (λ_{Cu} and λ_{Fc}). Indeed, ligand coordination/uncoordination processes as well as geometric changes often induce significant reorganizational energies for the Cu(II)/Cu(I) electron exchange. For ferrocenyl systems, this energy is much lower due to the small amplitude of the inner contribution (typically 0.03 eV [60]).

Table 7 allows the comparison between Cu(**2-4**)complexes for the Fc⁺/Fc. Hence a large drop of k^0 (90 to 50 s⁻¹) is observed as the alkyl spacer length of the triazole arm is increased (methyl to hexyl). To better understand this variation, we based our analysis on the general expression of the standard rate constant for alkanethiol SAMs [60–62]: the equation (12) predicts an exponential decrease of k^0 with the number of methylene motifs (n_{CH_2}) or the distance vs the electrode surface (r), the electron transfer occurring by direct tunneling between the surface and the redox species :

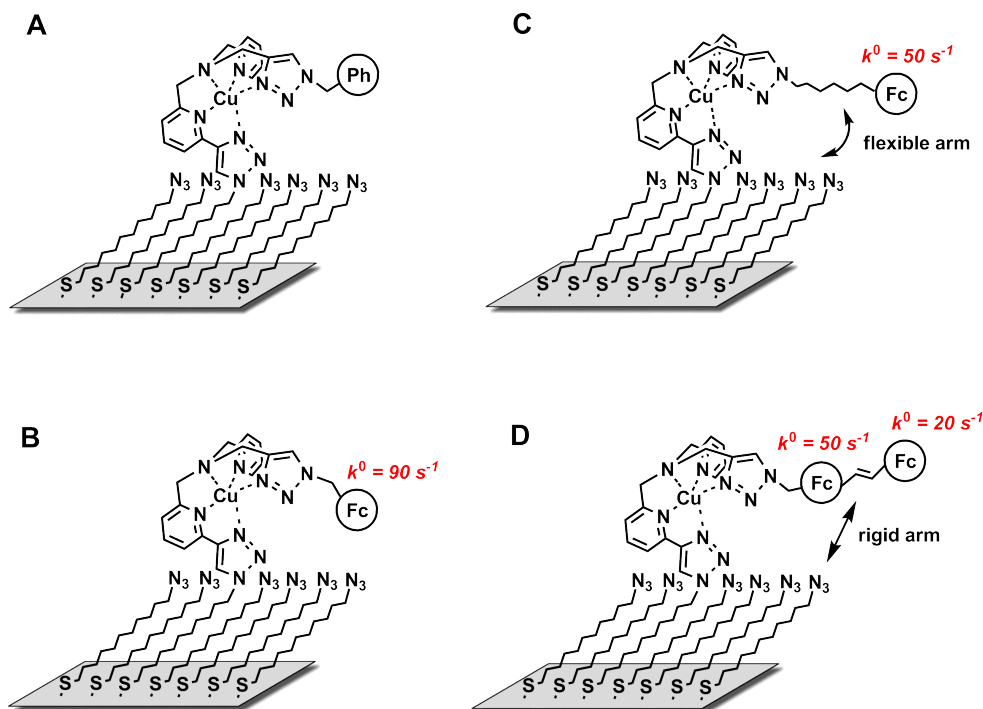
$$k^0 = k_{r=0}^0 \exp[-\beta_r r] = k_{n_{CH_2}=0}^0 \exp[-\beta_{n_{CH_2}} n_{CH_2}] \quad (12)$$

Table 7: Standard rate constant values (k^0) for the grafted $[\text{Cu}^{\text{II}}(\mathbf{1-4})(\text{L})_n]^{2+}$, $[\text{Cu}^{\text{II}}(6\text{eTMPA})(\text{L})_n]^{2+}$ and ethynylferrocene complexes from the analysis of the cyclic voltammetry data obtained in a 0.05 M buffer acetate solution (pH=4.5) + NaBF_4 0.05 M (based on Laviron's model [58])

Complex	k^0 /s ⁻¹	
	$\text{Cu}^{\text{II/I}}$	Fc^+/Fc
$[\text{Cu}^{\text{II}}\mathbf{1}(\text{L})_n]^{2+}$	4	
$[\text{Cu}^{\text{II}}\mathbf{2}(\text{L})_n]^{2+}$	4	90
$[\text{Cu}^{\text{II}}\mathbf{3}(\text{L})_n]^{2+}$	3	50
$[\text{Cu}^{\text{II}}\mathbf{4}(\text{L})_n]^{2+}$	2	50 ^a , 20 ^b
$[\text{Cu}^{\text{II}}(6\text{eTMPA})(\text{L})_n]^{2+}$	10	
EthynylFc		300

^a Di-substituted ferrocenyl unit;

^b Mono-substituted ferrocenyl unit.



Scheme 3: Representation of the Cu complexes grafted on the modified Au electrode: A) $[\text{Cu}^{\text{II}}\mathbf{1}(\text{L})_n]^{2+}$; B) $[\text{Cu}^{\text{II}}\mathbf{2}(\text{L})_n]^{2+}$; C) $[\text{Cu}^{\text{II}}\mathbf{3}(\text{L})_n]^{2+}$; D) $[\text{Cu}^{\text{II}}\mathbf{4}(\text{L})_n]^{2+}$; (L is not represented).

$[k_{x=0}^0]$ is the extrapolated standard rate constant value for $x=0$, β_x is the exponential decay coefficient for $x = r, n_{\text{CH}_2}$.

The exponential decay coefficient β_x is dependent on the redox system features, as well as the length of the alkanethiol chain (or electrode distance) [60, 62]. The equation (12) can thus be expressed as a function of an electron coupling factor (V_x) and the reorganizational energy λ [63], both varying with n_{CH_2} (or r):

$$k^0 = \frac{2\pi}{\hbar} \sqrt{\frac{1}{4\pi\lambda k_{\text{B}}T}} \exp\left[-\frac{\lambda}{4k_{\text{B}}T}\right] |V_x|^2 \quad (13)$$

[\hbar is the Dirac constant, k_{B} is the Boltzmann constant.]

The equation (13) predicts that a decrease of k^0 for Cu-**3** vs Cu-**2** may originate from the increase of the length which affects both the coupling factor (decrease) and the reorganizational energy (increase).

The comparison of the k^0 values obtained for the terminal ferrocenyl unit in Cu-**3** ($k^0 = 50 \text{ s}^{-1}$) and Cu-**4** ($k^0 = 20 \text{ s}^{-1}$) clearly demonstrates that the electron transfer is slower for Cu-**4** than for Cu-**3**. If one assumes that the length between the Fc and the triazole units is similar in both cases, this observation indicates that the conjugated arm in Cu-**4** is not involved in the electron transfer reaction to the terminal Fc. As a consequence, the lowest k^0 value obtained for Cu-**4** may be due to an increase of the distance between the terminal ferrocenyl group and the electrode (Scheme 3). The rigidity of the spacer seems thus to disfavor the electron transfer kinetics in that specific case. Moreover, the k^0 value obtained for the monosubstituted ferrocenyl group in Cu-**4** is significantly lower than that obtained for the disubstituted moiety ($k^0 = 20 \text{ s}^{-1}$ and 50 s^{-1} respectively). Assuming that the electron transfer reaction occurs via a direct tunneling process, this result indicates that both groups are not located at the same distance from the electrode surface, the disubstituted group being the closest.

4. Conclusion

In this study, two novel ligands bearing a ferrocenyl-based triazolyl arm linked to a 6eBMPA core have been synthesized. The complexation by Cu(II) was shown to induce a significant variation of the spectroscopic and voltammetric features of the ferrocene unit(s) depending on the spacer length and type (partial saturation). The diferrocenyl Cu(II) complex has been mono-electronically oxidized by exhaustive electrolysis in acetonitrile. The resulting mixed-valence complex is stable and belongs to the class II (moderate coupling) in the Robin-Day classification. The immobilization of these systems as SAMs on azidoundecanethiol modified gold electrode has been successfully operated by using the "self-induced electroclick" procedure. All grafted complexes display quasi-reversible responses in voltammetry in aqueous media and surface coverage values which are inversely proportional to their size. The standard potential related to the Cu-6eBMPA core does not vary with the triazole arm. However, the properties of the ferrocenyl unit(s) are significantly affected in thermodynamic and kinetic terms. In particular, our voltammetric studies show that the nature of the spacer on the ferrocenyl triazole part plays a significant role in the rate of charge transport by direct tunneling from (or to) the electrode. At last, the diferrocenyl complex described in our studies offers many interesting properties in terms of molecular QCA: (i) a little conjugation between Fc units, which is favorable to charge localization, (ii) a facile and controlled

immobilization onto azido modified surfaces by simple reduction of the Cu center, (iii) a mixed-valence complex with good stability in acetonitrile. Beyond the remarkable properties of the diferrocenyl Cu-4 complex, we hope that our methodology based on the self-induced electroclick property will serve for the immobilization of analogous systems in a more controlled way.

Acknowledgments. This research was supported by the CNRS, the Ministère de la Recherche et de l'Enseignement Supérieur (MESR grant for C.O.) and Agence National pour la Recherche (ANR-BLAN-7141).

Appendix. Supplementary Materials Ligand syntheses and characterization, spectroscopic and voltammetric data for Cu complexes.

References

- [1] T. Kurita, Y. Nishimori, F. Toshimitsu, S. Muratsugu, S. Kume, H. Nishihara, J. Am. Chem. Soc. 132 (2010) 4524–4525.
- [2] K. Seo, A. V. Konchenko, J. Lee, G. S. Bang, H. Lee, J. Am. Chem. Soc. 130 (2008) 2553–2559.
- [3] K. Terada, H. Nakamura, K. Kanaizuka, M. Haga, Y. Asai, T. Ishida, ACS Nano 6 (2012) 1988–1999.
- [4] J. Madoz, B. A. Kuznetsov, F. J. Medrano, J. L. Garcia, V. M. Fernandez, J. Am. Chem. Soc. 119 (1997) 1043–1051.
- [5] J. P. Collman, N. K. Devaraj, R. A. Decreau, Y. Yang, Y. L. Yan, W. Ebina, T. A. Eberspacher, C. E. D. Chidsey, Science 315 (2007) 1565–1568.
- [6] J. J. Concepcion, J. W. Jurss, M. K. Brennaman, P. G. Hoertz, A. O. T. Patrocinio, N. Y. M. Iha, J. L. Templeton, T. J. Meyer, Acc. Chem. Res. 42 (2009) 1954–1965.
- [7] W. J. Youngblood, S. H. A. Lee, Y. Kobayashi, E. A. Hernandez-Pagan, P. G. Hoertz, T. A. Moore, A. L. Moore, D. Gust, T. E. Mallouk, J. Am. Chem. Soc. 131 (2009) 926–927.
- [8] A. L. Eckermann, D. J. Feld, J. A. Shaw, T. J. Meade, Coord. Chem. Rev. 254 (2010) 1769–1802.
- [9] C. Vericat, M. E. Vela, G. Benitez, P. Carro, R. C. Salvarezza, Chem. Soc. Rev. 39 (2010) 1805–1834.
- [10] J. C. Love, L. A. Estroff, J. K. Kriebel, R. G. Nuzzo, G. M. Whitesides, Chem. Rev. 105 (2005) 1103–1169.
- [11] N. K. Devaraj, R. A. Decreau, W. Ebina, J. P. Collman, C. E. D. Chidsey, J. Phys. Chem. B 110 (2006) 15955–15962.
- [12] D. J. Feld, H. T. Hsu, A. L. Eckermann, T. J. Meade, Langmuir 28 (2012) 939–949.
- [13] B. Kim, J. M. Beebe, C. Olivier, S. Rigaut, D. Touchard, J. G. Kushmerick, X. Y. Zhu, C. D. Frisbie, J. Phys. Chem. C 111 (2007) 7521–7526.
- [14] N. Tuccitto, V. Ferri, M. Cavazzini, S. Quici, G. Zhavnerko, A. Licciardello, M. A. Rampi, Nat. Mater. 8 (2009) 41–46.
- [15] H. Qi, S. Sharma, Z. H. Li, G. L. Snider, A. O. Orlov, C. S. Lent, T. P. Fehlner, J. Am. Chem. Soc. 125 (2003) 15250–15259.

- [16] V. Arima, M. Iurlo, L. Zoli, S. Kumar, M. Piacenza, F. Della Sala, F. Matino, G. Maruccio, R. Rinaldi, F. Paolucci, M. Marcaccio, P. G. Cozzi, A. P. Bramanti, *Nanoscale* 4 (2012) 813–823.
- [17] P. Day, M. B. Robin, *Adv. Inorg. Chem. Radiochem.* 10 (1967) 247–422.
- [18] C. S. Lent, B. Isaksen, M. Lieberman, *J. Am. Chem. Soc.* 125 (2003) 1056–1063.
- [19] J. Y. Jiao, G. J. Long, F. Grandjean, A. M. Beatty, T. P. Fehlner, *J. Am. Chem. Soc.* 125 (2003) 7522–7523.
- [20] S. B. Braun-Sand, O. Wiest, *J. Phys. Chem. B* 107 (2003) 9624–9628.
- [21] S. B. Braun-Sand, O. Wiest, *J. Phys. Chem. A* 107 (2003) 285–291.
- [22] Z. H. Li, A. M. Beatty, T. P. Fehlner, *Inorg. Chem.* 42 (2003) 5707–5714.
- [23] Z. H. Li, T. P. Fehlner, *Inorg. Chem.* 42 (2003) 5715–5721.
- [24] J. Y. Jiao, G. J. Long, L. Rebbouh, F. Grandjean, A. M. Beatty, T. P. Fehlner, *J. Am. Chem. Soc.* 127 (2005) 17819–17831.
- [25] B. Schneider, S. Demeshko, S. Dechert, F. Meyer, *Angew. Chem. Int. Ed.* 49 (2010) 9274–9277.
- [26] C. Orain, N. Le Poul, A. Gomila, J. M. Kerbaol, N. Cosquer, O. Reinaud, F. Conan, Y. Le Mest, *Chem. Eur. J.* 18 (2012) 594–602.
- [27] A. Gomila, N. Le Poul, N. Cosquer, J. M. Kerbaol, J. M. Noel, M. T. Reddy, I. Jabin, O. Reinaud, F. Conan, Y. Le Mest, *Dalton Trans.* 39 (2010) 11516–11518.
- [28] M. Merkel, D. Schnieders, S. M. Baldeau, B. Krebs, *Eur. J. Inorg. Chem.* (2004) 783–790.
- [29] J. M. Casas-Solvas, A. Vargas-Berenguel, L. F. Capitan-Vallvey, F. Santoyo-Gonzalez, *Org. Lett.* 6 (2004) 3687–3690.
- [30] G. Colombano, C. Travelli, U. Galli, A. Caldarelli, M. G. Chini, P. L. Canonico, G. Sorba, G. Bifulco, G. C. Tron, A. A. Genazzani, *J. Med. Chem.* 53 (2010) 616–623.
- [31] J. P. Collman, N. K. Devaraj, C. E. D. Chidsey, *Langmuir* 20 (2004) 1051–1053.
- [32] Y. G. Lee, G. M. Morales, L. P. Yu, *Angew. Chem. Int. Ed.* 44 (2005) 4228–4231.
- [33] J. A. Mata, E. Peris, *J. Chem. Soc. Dalton Trans.* (2001) 3634–3640.
- [34] U. T. Muellerwesterhoff, Z. Yang, G. Ingram, *J. Organomet. Chem.* 463 (1993) 163–167.
- [35] M. F. Abasiyanik, M. Senel, *J. Electroanal. Chem.* 639 (2010) 21–26.
- [36] E. Lieber, C. N. R. Rao, T. S. Chao, C. W. W. Hoffman, *Anal. Chem.* 29 (1957) 916–918.
- [37] D. W. Hall, C. D. Russell, *J. Am. Chem. Soc.* 89 (1967) 2316–2322.
- [38] A. C. Ribou, J. P. Launay, M. L. Sachtleben, H. Li, C. W. Spangler, *Inorg. Chem.* 35 (1996) 3735–3740.
- [39] G. Ferguson, C. Glidewell, G. Opromolla, C. M. Zakaria, P. Zanello, *J. Organomet. Chem.* 517 (1996) 183–190.
- [40] N. Camire, U. T. Mueller-Westerhoff, W. E. Geiger, *J. Organomet. Chem.* 637 (2001) 823–826.
- [41] Y. J. Chen, D. S. Pan, C. F. Chiu, J. X. Su, S. J. Lin, K. S. Kwan, *Inorg. Chem.* 39 (2000) 953–958.
- [42] B. J. Hathaway, D. E. Billing, *Coord. Chem. Rev.* 5 (1970) 143–207.
- [43] S. K. Kang, H. S. Kim, Y. I. Kim, *Bull. Korean Chem. Soc.* 25 (2004) 1959–1962.
- [44] K. Jeyasubramanian, S. Thambidurai, S. K. Ramalingam, R. Murugesan, *J. Inorg.*

- Biochem. 72 (1998) 101–107.
- [45] A. A. Gewirth, S. L. Cohen, H. J. Schugar, E. I. Solomon, *Inorg. Chem.* 26 (1987) 1133–1146.
- [46] P. F. H. Schwab, J. R. Smith, J. Michl, *Chem. Rev.* 105 (2005) 1197–1279.
- [47] P. Aguirre-Etcheverry, D. O’Hare, *Chem. Rev.* 110 (2010) 4839–4864.
- [48] S. Barlow, D. O’Hare, *Chem. Rev.* 97 (1997) 637–669.
- [49] M. J. Powers, T. J. Meyer, *J. Am. Chem. Soc.* 100 (1978) 4393–4398.
- [50] W. Kaim, A. Klein, M. Glockle, *Acc. Chem. Res.* 33 (2000) 755–763.
- [51] P. F. Hapiot, L. D. Kispert, V. V. Konovalov, J. M. Saveant, *J. Am. Chem. Soc.* 123 (2001) 6669–6677.
- [52] B. S. Brunschwig, C. Creutz, N. Sutin, *Chem. Soc. Rev.* 31 (2002) 168–184.
- [53] N. S. Hush, *Electrochim. Acta* 13 (1968) 1005–1023.
- [54] N. S. Hush, *Coord. Chem. Rev.* 64 (1985) 135–157.
- [55] A. Caballero, A. Espinosa, A. Tarraga, P. Molina, *J. Org. Chem.* 72 (2007) 6924–6937.
- [56] J. P. Collman, N. K. Devaraj, T. P. A. Eberspacher, C. E. D. Chidsey, *Langmuir* 22 (2006) 2457–2464.
- [57] A. J. Bard, L. R. Faulkner, *Electrochemical Methods: Fundamentals and Applications*, 2nd ed., Wiley, 2001.
- [58] E. Laviron, *J. Electroanal. Chem.* 101 (1979) 19–28.
- [59] E. Laviron, L. Roullier, *J. Electroanal. Chem.* 115 (1980) 65–74.
- [60] J. F. Smalley, S. W. Feldberg, C. E. D. Chidsey, M. R. Linford, M. D. Newton, Y. P. Liu, *J. Phys. Chem.* 99 (1995) 13141–13149.
- [61] C. E. D. Chidsey, *Science* 251 (1991) 919–922.
- [62] K. Weber, L. Hockett, S. Creager, *J. Phys. Chem. B* 101 (1997) 8286–8291.
- [63] C. P. Hsu, R. A. Marcus, *J. Chem. Phys.* 106 (1997) 584–598.